European Journal of Medicinal Chemistry 73 (2014) 8–17

Contents lists available at ScienceDirect

European Journal of Medicinal Chemistry

journal homepage: http://www.elsevier.com/locate/ejmech

Original article

In vitro cytotoxicity studies of palladacyclic complexes containing the symmetric diphosphine bridging ligand. Studies of their interactions with DNA and BSA

Kazem Karami [a,*], Mahboubeh Hosseini-Kharat [a], Hojjat Sadeghi-Aliabadi [b], Janusz Lipkowski [c], Mina Mirian [d]

[a] Department of Chemistry, Isfahan University of Technology, Isfahan 84156/83111, Iran
[b] Department of Pharmaceutical Chemistry, Isfahan University of Medical Sciences, Isfahan, Iran
[c] Institute of Physical Chemistry, Polish Academy of Sciences, Kasprzaka 44/52, 01-224 Warsaw, Poland
[d] Department of Molecular Medicine, Isfahan University of Medical Sciences, Isfahan, Iran

ARTICLE INFO

Article history:
Received 16 October 2013
Received in revised form
18 November 2013
Accepted 24 November 2013
Available online 12 December 2013

Keywords:
Palladacyclic complex
FS-DNA binding
BSA binding
Cytotoxicity
Crystal structure

ABSTRACT

The reactions between $[Pd_2\{(C,N)-C_6H_4CH_2NH(Et)\}_2(\mu\text{-}X)_2]$ (X = Cl or Br) and 1,2-bis(diphenylphosphino)ethane (dppe) in the 1:1 molar ratio resulted in the dppe-bridged Pd(II) complexes, $[Pd_2\{(C,N)-C_6H_4CH_2NH(Et)\}_2(\mu\text{-dppe})(Cl)_2]$ (**1**) and $[Pd_2\{(C,N)-C_6H_4CH_2NH(Et)\}_2(\mu\text{-dppe})(Br)_2]$ (**2**), respectively, which were characterized by elemental analyses, infrared (IR), ^{1}H- and $^{31}P\{^1H\}$ NMR spectroscopy. The molecular structure of **1** was determined by single-crystal X-ray diffraction. *In vitro* cytotoxicity of **1**, **2**, dppe, $PhCH_2NH(Et)$ and cisplatin were carried out against four human tumor cell lines. The interactions of complexes towards DNA and protein are investigated. The results suggested that both complexes could interact with *FS*-DNA through the intercalation mode. Moreover, the reactivity towards BSA revealed that the microenvironment and the secondary structure of BSA were changed in the presence of Pd(II) complexes.

1. Introduction

To date, cisplatin and its analogs are some of the most effective chemotherapeutic agents in clinical use as the first line of treatment in testicular and ovarian cancers [1–6]. Furthermore, these analogs are increasingly used against other tumors, such as cervical, bladder and head/neck tumors. Unfortunately, they have several major side effects. Cumulative toxicities of nephrotoxicity, ototoxicity and tumor resistance related to them have stimulated the search for other antitumor-active metal complexes with improved pharmacological properties [7–12].

Mechanistic investigations of the mechanism of action of Pt(II) anticancer drugs, represent that their Pd(II) analogs are suitable model compounds since they exhibit ca. 10^4–10^5 times higher reactivity, whereas their structural and equilibrium behavior are very similar [13]. Among palladium(II) complexes, special attention has been paid to metallacycle complexes with nitrogen donor ligands, such as various alkyl and aryl substituted amines and imines, azo, hydrazo and heterocyclic compounds. The chelate ring generally possesses three to seven members, with the five-membered ring being most favored. These compounds are used successfully in organic synthesis [14–16], homogeneous and heterogeneous catalysis [17–19], asymmetric synthesis [20], photochemistry [21], optical resolution [22,23], and are rather promising as liquid crystals [24,25] and potential biologically active materials [26–30].

In the development of new such metal-based therapeutics, detailed studies on the interactions between DNA and transition-metal complexes is needed [31]. Depending on the exact nature of the metal and ligand, the complexes can bind with nucleic acid covalently or non-covalently [32,33]. Non-covalent interactions between transition-metal complexes and DNA can occur by intercalation, groove binding, or external electrostatic binding. Therefore, the study on the interaction of the transition metal complexes with DNA is of great significance for the design of new drugs and their application.

It has been found that some ortho-metalated species may bind to DNA by means of intercalative or monofunctional covalent

* Corresponding author. Tel.: +98 3113913239; fax: +98 3113912350.
E-mail addresses: karami@cc.iut.ac.ir (K. Karami), m.hosseinikharat@ch.iut.ac.ir (M. Hosseini-Kharat).

0223-5234/$ – see front matter © 2013 Elsevier Masson SAS. All rights reserved.
http://dx.doi.org/10.1016/j.ejmech.2013.11.042

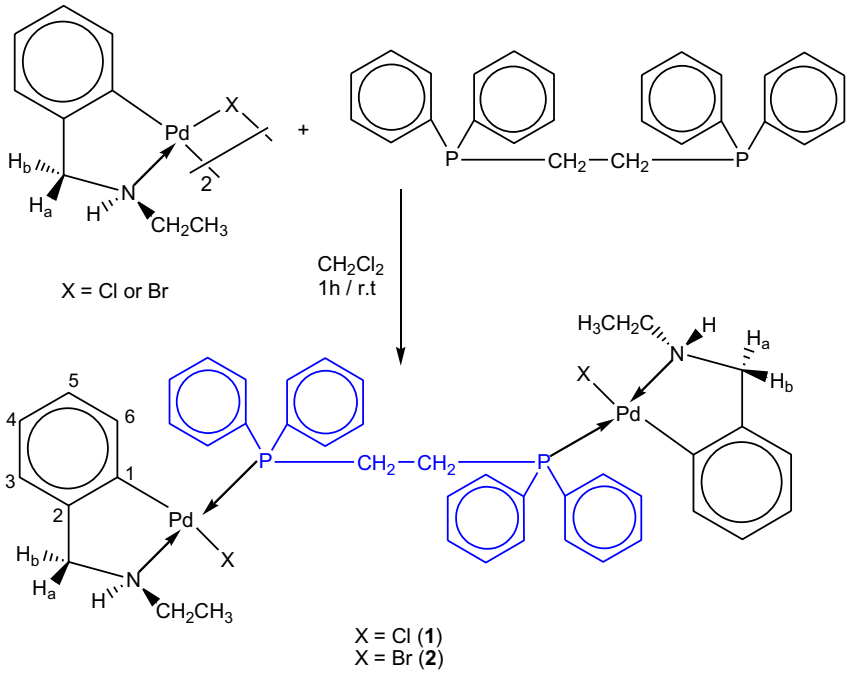

Scheme 1. Synthesis of the dppe-bridged palladacyclic complexes **1** and **2**.

interactions [34–36]. In case of palladacycles, proving that their intercalative mode of cytotoxic action is strictly related to the presence of a planar and highly stable aromatic metallacycle [37,38]. It was also reported that some cyclopalladated complexes containing planar structures such as aromatic and aliphatic amines exhibit cytotoxic effects against some tumor cells producing intercalative lesion on DNA [39,40], which drew our attention to study the biological activity of amine palladacycles in the form of biphosphinic complexes **1** and **2** (Scheme 1).

On the other hand, investigation on the effect of metal ions on drug–protein binding is useful to understand the transport and mechanism of the drug in the body [41,42]. Bovine serum albumin (BSA) is a protein with hydrophobic patches that could be the initial targets of their association to biomolecules [43]. Formation of a stable drug–protein complex can exert important effect on the distribution, free concentration and metabolism of the drug in the bloodstream. Thus the drug–albumin complex may be considered as a model for gaining fundamental insights into the drug–protein interactions [44,45].

Enlightened by the above-mentioned facts, it is necessary to design and synthesize new palladium complexes to evaluate their cytotoxicity and reactivity towards DNA and protein. Recently, much efforts have been devoted to the design and synthesis of new Pd(II) complexes and investigate their biological properties. Nevertheless, the studies on the interaction of cyclopalladated complexes with DNA and BSA are very limited.

Regarding to these facts and as a continuation of our ongoing program in the field of design and synthesis of new cyclopoalladated complexes, in this report, two new cyclopalladate–dppe complexes **1** and **2**, were synthesized and fully characterized. The detailed structure of **1** was also determined by X-ray single crystal analysis. We have evaluated the *in vitro* cytotoxic potential (IC_{50}) of the compounds **1** and **2** against the human cervix carcinoma (Hela), colon cancer (HT-29), leukemia cancer (K562) and human breast carcinoma (MCF-7) tumor cell lines. The interactions of the palladacyclic complexes with fish sperm DNA (*FS*-DNA) are investigated by UV absorption and fluorescence spectra. Furthermore, the protein binding ability has been monitored by UV absorption and tryptophan fluorescence quenching experiment in the presence of the complexes using BSA as a model protein.

2. Results and discussion

2.1. Synthesis and spectroscopic characterization

The reactions of the starting material $[Pd_2\{(C,N)-C_6H_4CH_2NH(Et)\}_2(\mu\text{-}X)_2]$ (X = Cl or Br) [46,47] with $Ph_2PCH_2CH_2PPh_2$ (dppe) in a 1:1 molar ratio give the complexes **1** and **2** in good yields. The preparation process of the complexes is very simple, and only one type of compound could be detected by the occurrence of only one precipitate, after the mixture of reactants was stirred at room temperature. This compound was determined as μ-dppe dinuclear palladium complex of the type *trans-**N**,**P***-$[Pd_2\{(C,N)-C_6H_4CH_2NH(Et)\}_2(\mu\text{-dppe})(X)_2]$ (X = Cl (**1**)) or (X = Br (**2**)), in which the symmetric bidentate ligand dppe bridges two identical cyclopalladated units. Both complexes were isolated as white solids, stable at room temperature, soluble in chlorinated solvents such as CH_2Cl_2, $CHCl_3$ and polar, aprotic solvent like DMSO (dimethylsulfoxide). Formation of isolated complexes has been confirmed on the basis of characteristic bands in the IR spectra, elemental analysis, resonance signals in the ^1H-, and $^{31}P\{^1H\}$ NMR, and single crystal X-ray crystallography.

The IR spectra of the complexes showed typical bands at 3193, 3205 cm^{-1}, 3048, 3049 cm^{-1}, 2962, 2966 cm^{-1}, 1100, 1101 $cm^{-1}$and 521, 522 cm^{-1}assigned to ν(N–H), ν(C–H Ph), ν(C–H alph), ν(C–P) and ν(Pd–P) for **1** and **2**, respectively.

The ^1H NMR spectra of **1** and **2** showed that these compounds represent a molecular structure with an apparent center of inversion, which divided the molecules into two symmetrical parts. This is in agreement with the structures proposed for these compounds with symmetric diphosphine ligand i) bridging the two palladium(II) centers and ii) coordinated to the cyclopalladated units with *trans-**N**,**P*** stereochemistry.

The $^{31}P\{^{1}H\}$ NMR spectra of **1** and **2** exhibited singlets at $\delta = 37.3$ and 36.7 ppm, respectively, as expected for the proposed structures. Moreover, in the ^{1}H NMR spectra, in according with the presence of aromatic rings in the bridging ligand close to the H_6 protons, these protons are shifted upfield in relation to the free ligand. Interestingly, the H_6 protons of **1** and **2** were virtually coupled with the two phosphorus atoms of the dppe bridging ligands, and afforded broad signals (Fig. 1). Similar behavior has already been observed for other related complexes [48].

2.2. Molecular structure of *1*

Complex **1** has been characterized in the solid phase by a single crystal X-ray diffraction study. Suitable crystals of **1** were obtained by slow diffusion of hexane into a CH_2Cl_2 solution. An ORTEP view of the dinuclear complex **1** is shown in Fig. 2. Relevant crystallographic data and structure refinement details are listed in Table 1. Selected bond lengths and angles are listed in Table 2.

This compound crystallized in the monoclinic space group *Pn* with $Z = 2$. The four coordinated palladium(II) is bonded to an *ortho*-carbon atom of the benzylamine ring, a nitrogen atom of the amine group and a chloro group *trans*-positioned to the carbopalladated site. A phosphorus atom from the diphosphine ligand, which bridges the two metal atoms, completes the metal coordination sphere. The Pd1···Pd2 distance is 7.446 (19) Å, showing that the two metal atoms in the dimer are not directly bonded. As can be seen in the molecular structure, the symmetric bidentate phosphine bridges the two palladium(II) centers and is coordinated to the cyclopalladated units in a *trans-N,P* stereochemistry. The sum of angles around the palladium atom is 359.7°, with the distortion most noticeable in the somewhat reduced "bite" angle of the metalated moiety. The requirements of the five-membered rings force the bond angles C38–Pd1–N1 and C5–Pd2–N2 to 82.4(9)° and 83.1(8)°, respectively.

The square-planar coordination geometry of the palladium(II) metal is slightly tetrahedrally distorted, and the mean deviations from the least squares plane are only 0.030 Å, Pd1 and 0.087 Å, Pd2. This planar geometry makes the complex ideally suited for potential intercalation into DNA. The angles between the cyclopalladated rings and the central fragment P1–C1–C2–P2 is 61.60° and 72.91°, respectively. The torsion angle P1–C1–C2–P2 of 178.5(16)° deviates from the ideal value of 180°. This is because the molecule is not located in an inversion center of the crystal. The Pd–N bond lengths (2.102(19) and 2.123(14) Å) are longer than the sum of the covalent radii of Pd and N(sp^2) atoms (2.011 Å) [49] and is also slightly longer than the mean value of 2.07 Å observed for related cyclopalladated compounds [46,50]. This lengthening indicates a weakening of the Pd–N bond due to the great *trans* influence of the phosphorous atom from dppe ligand. In addition, The Pd–N

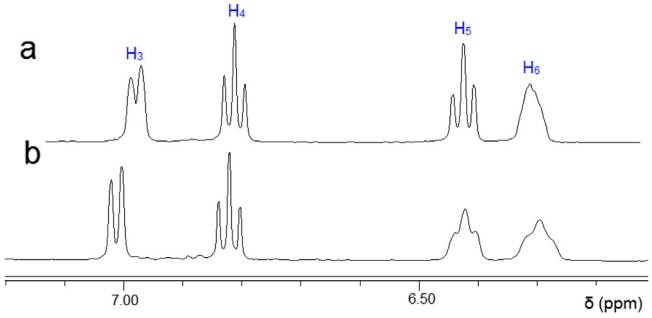

Fig. 1. The four aromatic protons of the cyclopalladated benzylamine moiety in the ^{1}H NMR spectra of **1** (a) and **2** (b).

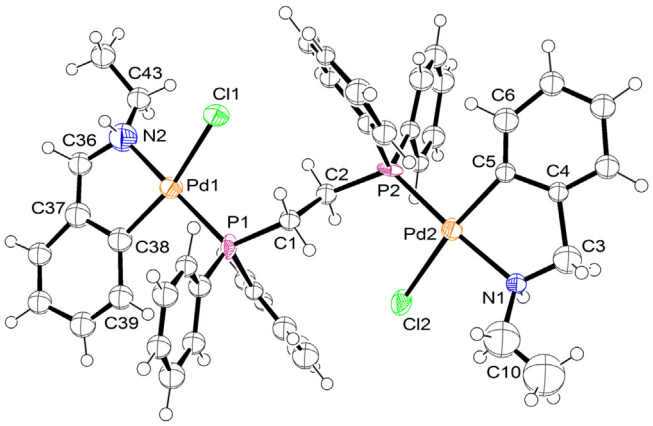

Fig. 2. ORTEP diagram for palladacyclic complex **1** with ellipsoids drawn at the 50% probability level.

distances are also longer than the analogous distances reported in other bridged biphosphinic palladacycles (2.086(5)–2.099(8) Å) [48,51]. The Pd–$C_{palladate}$ distances (2.02(3) and 1.99(2) Å) are shorter than the predicted value of 2.081 Å (based on the sum of the covalent radii for C(sp^2) and Pd, 0.771 and 1.31 Å, respectively) [49] but lies in the range of 1.983(2)–2.068(3) Å obtained for related complexes [29,46,48].

2.3. DNA-binding studies

2.3.1. Electronic absorption titration

Electronic absorption spectroscopy is one of the most useful techniques for DNA-binding studies of metal complexes. The absorption spectra of the two complexes in the absence and presence of *FS*-DNA are given in Fig. 3. The intense absorption bands around 235 nm reveal the intraligand π–π* transition of the coordinated groups. Addition of increasing amounts of *FS*-DNA resulted in a reduction in absorbency (hypochromism) without any shift in the absorption maxima in the UV spectra of the complexes. Normally, a compound binding to DNA through intercalation mode results in hypochromism with or without a small red or blue shift, due to a

Table 1
Crystallographic data and structure refinement details for **1**.

	1
Empirical formula	$C_{44}H_{48}Cl_2N_2P_2Pd$
Formula weight	950.57
T/K	100 (1)
Crystal system	Monoclinic
Space group	*Pn*
a/Å	11.9250(10)
b/Å	13.2650(10)
c/Å	13.4690(10)
α/°	90.00
β/°	108.344(8)
γ/°	90.00
V/Å^3	2022.33(3)
Z	2
μ (mm^{-1})	9.42
D_{cal}/Mg m^{-3}	1.587
F(000)	980
θ range/°	3.3–70.1
Independent reflections	4201
Data/restraints/parameters	4201/0/246
Goodness-of-fit on F^2	1.105
Final *R* indices	$R_1 = 0.0643$, $wR_2 = 0.1584$
R indices (all data)	$R_1 = 0.0793$, $wR_2 = 0.1733$
Largest difference peak and hole (e Å^{-3})	1.44, −1.20

Table 2
Selected bond lengths (Å), and angles (°) for **1**.

Atoms			
Bond lengths			
Pd1–Cl1	2.371(7)	Pd2–Cl2	2.404(7)
Pd1–P1	2.263(7)	Pd2–P2	2.253(7)
Pd1–N2	2.102(19)	Pd2–N1	2.123(14)
Pd1–C38	2.02(3)	Pd2–C5	1.99(2)
P1–C1	1.83(2)	P2–C2	1.89(2)
Bond angles			
C38–Pd1–N2	82.4(9)	C5–Pd2–N1	83.1(8)
C38–Pd1–P1	95.9(8)	C5–Pd2–P2	93.8(7)
P1–Pd1–Cl1	92.5(3)	P2–Pd2–Cl2	92.8(2)
N2–Pd1–Cl1	90.4(5)	N1–Pd2–Cl2	90.0(4)
N2–Pd1–P1	172.8(5)	N1–Pd2–P2	175.7(4)
C38–Pd1–Cl1	167.3(8)	C5–Pd2–Cl2	170.8(7)
C1–P1–Pd1	116.6(8)	C2–P2–Pd2	119.0(8)
P1–C1–C2	116.3(9)	P2–C2–C1	113.0(9)
C36–N2–Pd1	111.2(13)	C3–N1–Pd2	116.0(12)
C43–N2–Pd1	125.5(14)	C10–N1–Pd2	118.0(12)
Pd1–N2–C36–C37	3.3(15)	Pd2–N1–C3–C4	3.9(19)
C36–C37–C38–Pd1	9.(3)	C3–C4–C5–Pd2	−9.(2)
P1–Pd1–C38–C39	5.(2)	P2–Pd2–C5–C6	−3.(2)

strong stacking interaction between the planar aromatic chromophore of the compound and the base pairs of DNA [52,53]. Hence, the observed hypochromic effect in the intraligand band suggests that the new Pd(II) complexes are likely to bind to *FS*-DNA via intercalation mode. In order to compare the binding strength of the complexes, their intrinsic binding constants (K_b) were evaluated in accordance the method proposed by Wolfe et al. [54] using the equation:

$$[\mathrm{DNA}]/\left(\varepsilon_a - \varepsilon_f\right) = [\mathrm{DNA}]/\left(\varepsilon_b - \varepsilon_f\right) + 1/K_b\left(\varepsilon_b - \varepsilon_f\right)$$

where [DNA] is the concentration of DNA in the base pairs, ε_a is the apparent absorption coefficient corresponding to A_{obs}/[compound], ε_f is the extinction coefficient of the free compound and ε_b is the extinction coefficient of the compound when fully bound to DNA. The intrinsic binding constant K_b is determined by the ratio of slope to the *Y* intercept in plots of [DNA]/($\varepsilon_a - \varepsilon_f$) versus [DNA] (Fig. 3). The K_b values of **1** and **2** were calculated about 0.4×10^3 and 4.5×10^3 M^{-1}, respectively. The larger value of K_b for complex **2** indicates better binding with DNA for **2**.

From the values of binding constant (K_b), free energy (ΔG) of compound–DNA complex was calculated, using the following equation:

$$\Delta G = -RT \ln K_b$$

Binding constants are measure of compound–DNA complex stability while free energy indicates the spontaneity/non-spontaneity of compound–DNA binding. Free energies of **1** and **2** were evaluated as negative values (−18.84 and −20.84 KJ mol^{-1}, respectively) showing the spontaneity of compounds–DNA interaction. However, these results indicated that **2** binds to the DNA more spontaneously as compared to **1**.

2.3.2. EB displacement experiment

The Ethidium bromide (EB) displacement experiment was carried out to gain support for the mode of binding of the complex with DNA from absorption titration experiments. EB (3,8-diamino-5-ethyl-6-phenylphenanthrium bromide) is known to emit intense fluorescence in the presence of DNA due to its strong intercalation between the base pairs of DNA. It has been reported that the enhanced fluorescence can be quenched by the addition of the complex which can compete with EB to bind with DNA. This is a proof that complexes intercalate to base pairs of DNA [55,56]. The

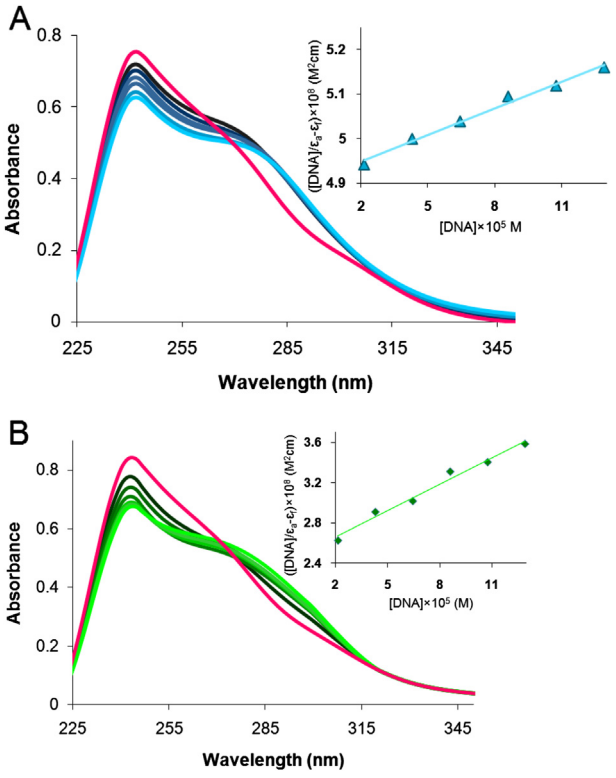

Fig. 3. Electronic spectra of **1** (A) and **2** (B) in buffer solution (5 mM Tris–HCl/10 mM NaCl at pH 7.2) upon addition of *FS*-DNA. [Complex] = 50 μM, [DNA] = 0–120 μM. Arrow shows the absorption intensities decrease upon increasing DNA concentration. Inset: Plots of [DNA]/($\varepsilon_a - \varepsilon_f$) vs. [DNA] for the titration of **1** and **2** with *FS*-DNA.

quenching extent of fluorescence of EB-DNA is used to determine the extent of binding between the complex and DNA. The emission spectra of EB bind to DNA in the absence and presence of Pd(II) complexes are given in Fig. 4. The addition of the complexes to DNA pretreated with EB cause an obvious reduction in the emission intensity. The observed decrease in the fluorescence intensity clearly indicates that the EB molecules are displaced from their DNA binding sites and are replaced by the compounds under investigation. From the spectral data, the quenching parameter can be analyzed according to the Stern–Volmer equation,

$$F_0/F = K_{sv}[Q] + 1$$

where F_0 is the emission intensity in the absence of compound, *F* is the emission intensity in the presence of compound, K_{sv} is the quenching constant, and [*Q*] is the concentration of the compound. The K_{sv} value is obtained as a slope from the plot of F_0/F versus [*Q*] (Stern–Volmer plot) (Fig. 4). The experimental results data (Table 3) suggest that both the complexes bind to DNA via intercalation but the complex **2** binds to DNA more strongly than the complex **1**, which is in agreement with the results observed from the electronic absorption spectra.

2.4. BSA binding study

Serum albumin (SA) is the most abundant protein in plasma and is involved in the transport of drugs, metal ions, and compounds through the bloodstream. BSA is the most extensively studied serum albumin, due to its structural homology with human serum albumin (HSA). Binding to these proteins may lead to loss or enhancement of the biological properties of the original drug, or provide paths for drug transportation. Since serum albumins are

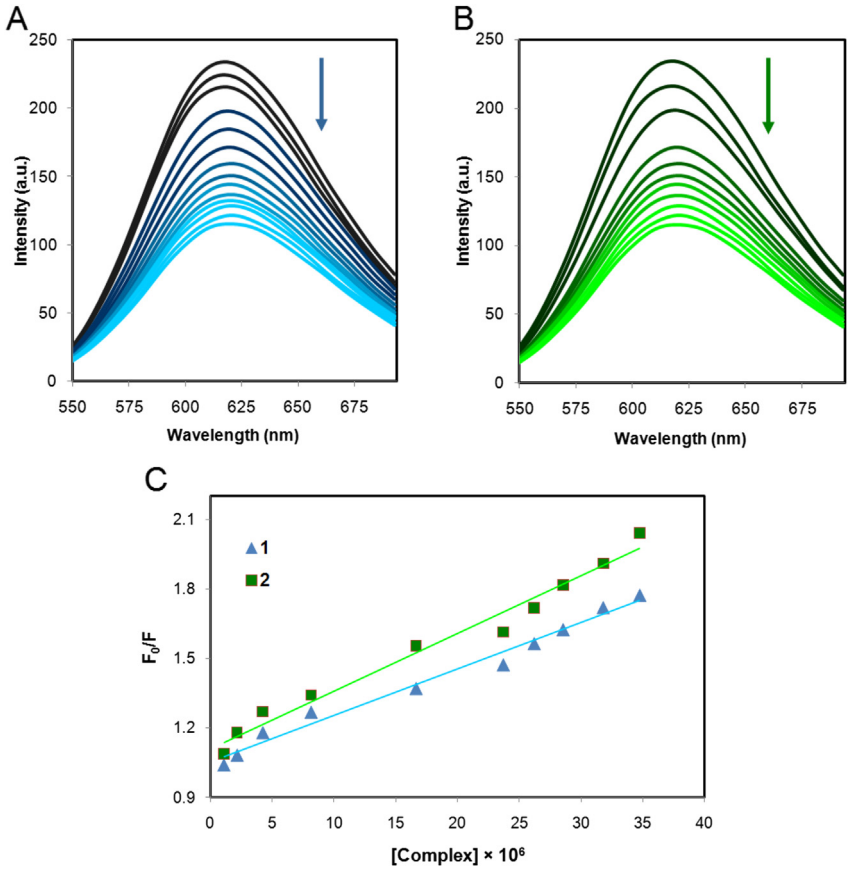

Fig. 4. The emission spectra of the DNA–EB system, in the presence of **1** (A) and **2** (B). [DNA] = 60 μM, [Complex] = 0–40 μM, [EB] = 2 μM. The arrow shows the emission intensity changes upon increasing complex concentration. Stern–Volmer plots of the EB-DNA fluorescence titration data of **1** and **2** (C).

well known to bind small aromatics, the possible binding interactions of **1** and **2** with BSA have been investigated by absorption and emission-titration experiments at room temperature.

2.4.1. UV absorption spectra of BSA in the presence of the complexes

UV absorption spectrum is a very simple and applicable method to explore the structural change and to know the complex formation in solution [57]. Fig. 5 shows the UV absorption spectra of BSA in the presence of different concentrations of the two complexes. As can be seen from this figure, BSA has two main absorption bands. One is located in the range of 220–240 nm, which is the skeleton absorption peak, and the other is at 278 nm, which is the absorption band of the aromatic amino acids (Trp, Tyr, and Phe). Fig. 5 indicates that upon adding the two complexes, the BSA skeleton absorption intensity in the range of 220–240 nm is increased and red-shifted. In addition, the maximum absorption at 278 nm is also enhanced with a blue shift (from 278 nm to 274 and 267 nm for **1** and **2**, respectively). This phenomenon indicates the interaction of BSA with the complexes [58]. It is well known that dynamic quenching only affects the excited state of fluorophore and does not change the absorption spectrum. However, the formation of non-fluorescence ground-state complex induced the change in absorption spectrum of fluorophore. Thus, possible quenching mechanism of BSA by **1** and **2** was a static quenching process [59,60].

2.4.2. Tryptophan quenching experiment

In order to further investigate the interaction of the two complexes with protein, the tryptophan emission-quenching experiments were carried out using BSA in the presence of the two complexes. Generally, the fluorescence of protein is caused by three intrinsic characteristics of the protein, namely tryptophan, tyrosine, and phenyl alanine residues. Actually, the intrinsic fluorescence of many proteins is mainly contributed by tryptophan alone. The emission intensity depends on the degree of exposure of the two tryptophan side chains [61], 134 and 212, to polar solvent. As already mentioned in the above section, quenching can occur by different mechanisms either by dynamic or static. Dynamic quenching refers to a process in which the fluorophore and the quencher come into contact during the transient existence of the excited state while the latter type of quenching refers to fluorophore–quencher complex formation in the ground state.

It can be seen from Fig. 6, the fluorescence emission intensities of BSA at 343 nm show moderate decreasing trend with increasing concentration of the two complexes, indicating that the interaction of the complexes with BSA could cause changes in protein secondary structure leading to changes in tryptophan environment of BSA [62].

In order to understand quantitatively the magnitude of the complexes to quench the emission intensity of BSA, the linear Stern–Volmer equation is also employed [57].

$$F_0/F = 1 + K_{sv}[Q] = 1 + K_q\tau_0[Q]$$

F_0 and F represent the fluorescence intensities in the absence and presence of quencher, respectively. K_{sv} is a linear Stern–Volmer quenching constant. K_q is the quenching rate constant of biomolecule, τ_0 is the average lifetime of the fluorophore without

Table 3
Quenching constant (K_{sv}), binding constant (K_{bin}), free energy (ΔG) and number of binding sites (n) for the interactions of **1** and **2** with *FS*-DNA.

Complex	K_{sv}/M^{-1}	K_{bin}/M^{-1}	$-\Delta G$/KJ mol^{-1}	n
1	2.1×10^4	9.4×10^2	16.96	0.67
2	2.6×10^4	3.3×10^3	20.07	0.81

quencher, the value of τ_0 of the biopolymer is 10^{-8} s, and [Q] is the concentration of quencher.

From the quenching plot of F_0/F versus [complex] (Fig. 6), K_{sv} and K_q of the two complexes are obtained from the slope. The calculated values of K_{sv} and K_q for the interaction of **1** and **2** with BSA are given in Table 4 and indicate good BSA binding propensity of the complexes with **2** exhibiting the higher protein-binding ability. The K_q values ($\sim 10^{12}$ M^{-1} s^{-1}) are higher than diverse kinds of quenchers for biopolymers fluorescence (2.0×10^{10} M^{-1} s^{-1}) indicating the existence of static quenching mechanism [63]. Therefore, the quenching of BSA fluorescence by the two complexes depended on the formation of the complex between the compounds and BSA.

2.4.3. Binding constants, number of binding sites and Gibbs free energy values

For the static quenching interaction, if it is assumed that there are similar and independent binding sites in the biomolecule, the binding constant (K_{bin}) and the number of binding sites (n) can be determined according to the Scatchard equation [64]:

$$\log[(F_0-F)/F] = \log K_{bin} + n \log[Q]$$

where K_{bin} is the binding constant for the complex-BSA or -DNA interactions and n is the number of binding sites per albumin or DNA molecule, which can be determined by the slope and the intercept of the double logarithm regression curves of log [$(F_0 - F)$/F] versus log [Q] (Figs. 7 and 8).

The results in Tables 3and 4 indicate that there are more binding sites on BSA than DNA for both complexes. Furthermore, $n < 1$ for compound–DNA complex implies only a binding site per two base pairs, giving evidences for an intercalation mode, since groove binding and electrostatic binding usually results in significantly higher binding site number [65,66].

The values of K_{bin} exhibit that there is interaction and the formation of complex between compounds and DNA or BSA. The binding constants of both complexes with DNA and BSA follow this order: **2**-BSA > **2**-DNA > **1**-BSA > **1**-DNA. These results are consistent with greater DNA or BSA binding affinity of **2**.

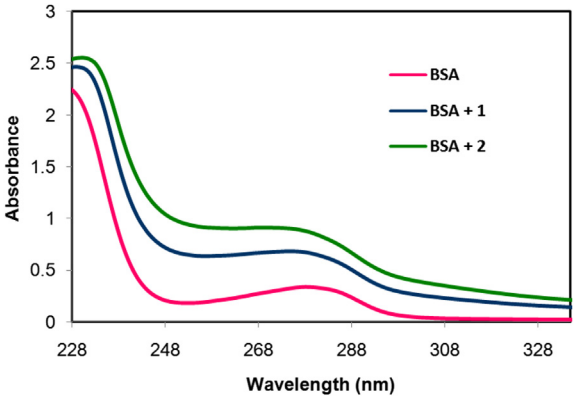

Fig. 5. UV absorption spectra of BSA (15 μM) in the absence and presence of complexes (10 μM) **1** and **2**.

From the binding constant data, the standard Gibbs free energy changes for **1** and **2** were also calculated, (Tables 3and 4). The negative values of ΔG through fluorescence results also supported the UV-results of free energy changes and indicated the spontaneity of the compound–DNA or BSA binding.

2.4.4. Energy transfer between the palladacyclic complexes and BSA

The importance of the energy transfer in biochemistry is that, the efficiency of transfer can be used to evaluate the distance, r, between the compound and tryptophan residues in the protein. According to the Foster's non-radioactive resonance energy transfer theory (FRET) [67], the effective energy transfer from donor to acceptor will occur when two molecules meet the following preconditions: (i) donor is a fluorophore; (ii) the overlap is enough between the fluorescence emission spectrum of the donor and UV–vis absorption spectrum of the acceptor; (iii) the distance between

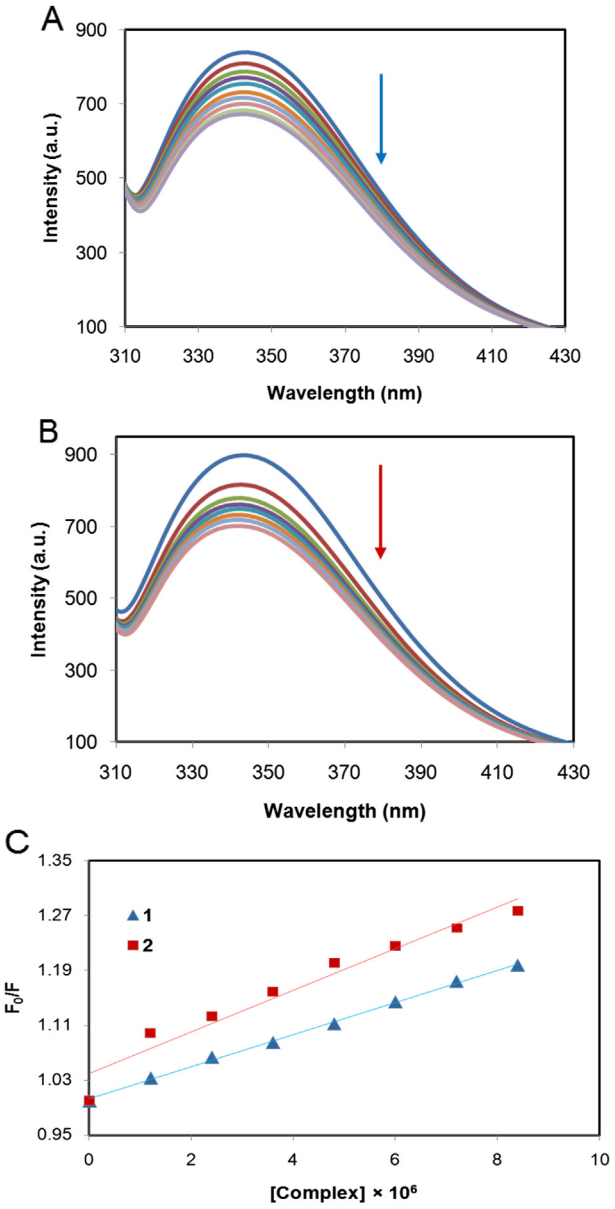

Fig. 6. Emission spectra of BSA upon the titration of **1** (A) and **2** (B) [BSA] = 6 μM, [Complex] = 0–10 μM. Arrow shows the change upon the increasing complex concentration. Plots of F_0/F vs. [complex] for the titration of the complexes to BSA (C).

Table 4
Quenching constant (K_{sv}), binding constant (K_{bin}), free energy (ΔG) and number of binding sites (n) for the interactions of **1** and **2** with BSA.

Complex	K_{sv}/M^{-1}	$K_q/M^{-1}\ s^{-1}$	K_{bin}/M^{-1}	$-\Delta G$/KJ mol^{-1}	n
1	2.3×10^4	2.3×10^{12}	1.6×10^3	18.27	0.74
2	3.1×10^4	3.1×10^{12}	1.02×10^4	22.86	0.92

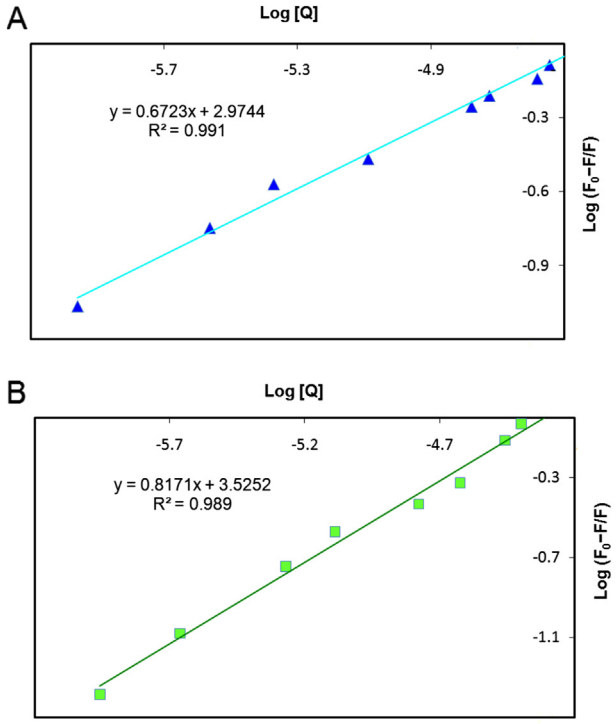

Fig. 7. Scatchard plots of log $[(F_0 - F)/F]$ vs log [Q] for determination of the complex-DNA binding constant and the number of binding sites on DNA for **1** (A) and **2** (B).

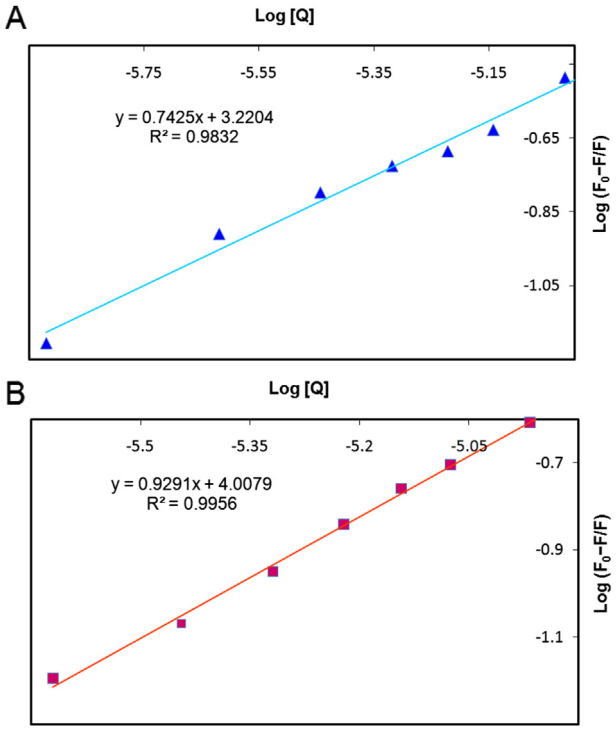

Fig. 8. Scatchard plots of log $[(F_0 - F)/F]$ vs log [Q] for determination of the complex-BSA binding constant and the number of binding sites on BSA for **1** (A) and **2** (B).

the donor and the acceptor is within 2–8 nm. The energy transfer effect is not only related to the distance between the donor (tryptophan residue) and acceptor, but also influenced by the critical energy transfer distance R_0. It is described by the following equations:

$$E = 1-(F/F_0) = \left[1 + (r/R_0)^6\right]^{-1}$$

$$R_0 = \left[8.79 \times 10^{-25} K^2 N^{-4} \Phi J\right]^{-6}$$

where R_0 is the critical energy transfer distance when the transfer efficiency is 50%, r is the distance between the acceptor and the donor, and E is the energy transfer efficiency. K is the spatial orientation factor of the dipole, N is refractive index of the medium, Φ is the fluorescence quantum yield of the donor, and the overlap integral (J) between the fluorescence emission spectrum of the donor and the absorption spectrum of the acceptor can be calculated using the equation below [68]:

$$J = \sum F(\lambda)\varepsilon(\lambda)\lambda^4 \Delta\lambda / \sum F(\lambda)\Delta\lambda$$

where $F(\lambda)$ is the fluorescence intensity of the fluorescent donor at some wavelength, $\varepsilon(\lambda)$ is the molar absorbance of the acceptor at the wavelength λ. Fig. 9 presents the overlap integral of the fluorescence emission spectra of BSA and the absorption spectra of Pd(II) complexes. In the present case, $K^2 = 2/3$, $N = 1.336$, and $\Phi = 0.15$ [69]. Hence, from the above equations we could calculate the following parameters: $J = 2.05 \times 10^{-15}\ M^{-1}\ cm^3$, $R_0 = 1.96$ nm, $E = 0.083$, and $r = 2.92$ nm for **1** and $J = 1.28 \times 10^{-14}\ M^{-1}\ cm^3$, $R_0 = 2.65$ nm, $E = 0.089$, and $r = 3.91$ nm for **2**. Obviously, the

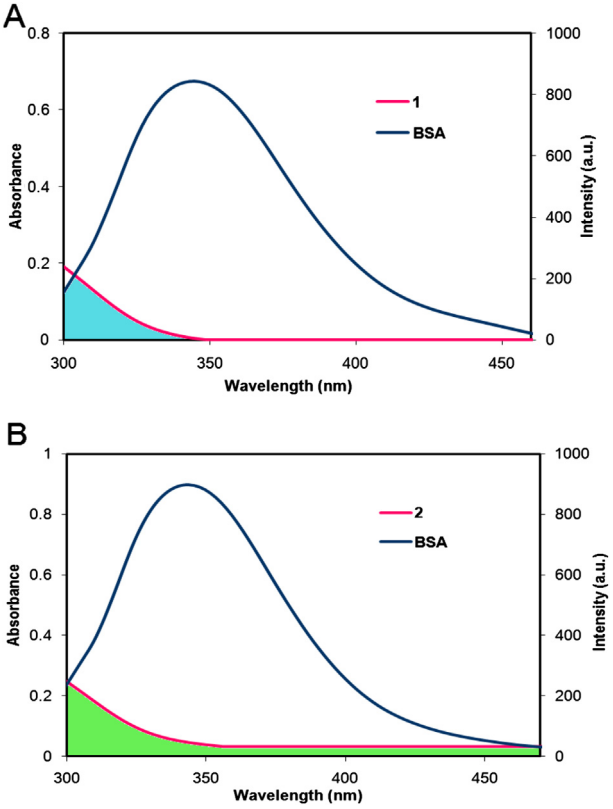

Fig. 9. Spectral overlaps of the absorption spectra of **1** (A) and **2** (B) with the fluorescence spectra of BSA.

Table 5
Cytotoxicity data (IC_{50}) of the dppe and *N*-benzyl ethylamine ligands and their palladium (II) complexes against human Hela, HT-29, K562 and MCF-7 tumor cell lines.

Compound	IC_{50} (μM) ± SD			
	Hela	HT-29	K562	MCF-7
dppe	>100	100 ± 0.02	100 ± 0.1	>100
N-Benzyl ethylamine	>100	100 ± 0.09	100 ± 0.07	100 ± 0.06
1	8.5 ± 0.4	7.5 ± 0.22	3.1 ± 0.02	7.5 ± 0.02
2	7.5 ± 0.6	5.3 ± 0.5	2.5 ± 0.51	7.5 ± 0.05
cisplatin	53.5 ± 1.4	41.2 ± 0.09	7.6 ± 0.07	5.2 ± 0.04

distance between each complex and BSA is less than 8 nm, and $0.5R_0 < r < 1.5R_0$, implying that the energy transfer from BSA to complexes occurred with high probability. The bigger r value compared with that of R_0 again indicated the presence of static quenching mechanism in the binding of two complexes to BSA [70].

2.5. Cytotoxic activity against human tumor cell lines

In vitro cytotoxicity of compounds was evaluated by means of the standard MTT-dye reduction assay which is a widely used method in biological evaluation. Recently, new metal complexes were assessed using this method [71,72]. The cytotoxic activity of the dppe and *N*-benzyl ethylamine ligands and their Pd(II) complexes were tested against human cervix carcinoma (Hela), colon cancer (HT-29), leukemia cancer (K562) and human breast carcinoma (MCF-7) tumor cell lines. The results are reported in Table 5 in terms of IC_{50} values (the concentration needed to inhibit 50% of the cellular proliferation). For comparison purposes, the cytotoxicity of cisplatin, a standard antitumor drug, was evaluated under the same conditions. As depicted in Table 5, compounds **1** and **2** exhibit high antiproliferative activity with IC_{50} values in the range 2–9 μM below those of cisplatin in three cell lines, which is a reflection of their good solubility and lipophilicity. The lipophilicity of the bridged complexes can be related to the presence of two bulky PPh_2 groups from dppe which facilitate transport through the cellular membranes. In addition, the dppe bridge leads to the more flexibility in the structures and makes more interactions with DNA.

It was also observed that **1** and **2** demonstrated a noticeable cytotoxicity against all cell lines when compared with the free ligands, implying that the biological activity is largely ascribed by the presence of the Pd(II) metal center. In addition, compound **2** exhibited a slightly higher toxicity than **1** against Hela, HT-29 and K562 cell lines (Fig. 10). These results suggest that the replacement of the chloride by the bromide ligand increased the cytotoxic activity of the Pd(II) compound in these three cell lines, as observed in the screening of other antitumor agents [73,74].

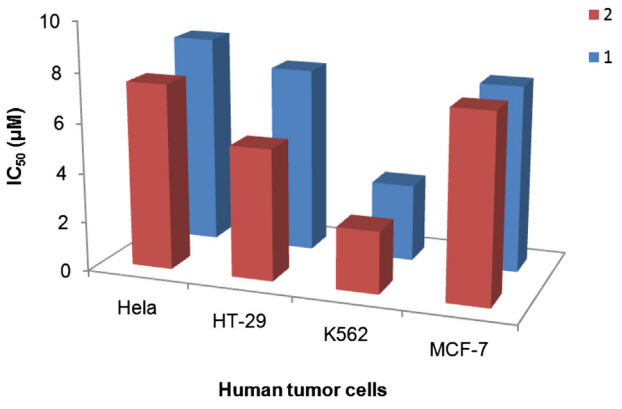

Fig. 10. *In vitro* cytotoxic activity of **1** and **2** against different human tumor cell lines.

3. Conclusion

Two new cyclopalladated compounds bearing biphosphinic ligand dppe have been described in this work. The single crystal X-ray crystallographic study of **1** revealed a slightly tetrahedrally distorted square planar geometry around the Pd(II) ion. The DNA-binding properties of the two complexes were explored by electronic absorption and fluorescence spectroscopy. The results suggested that both complexes could interact with *FS*-DNA through the intercalation mode and both follow the binding affinity order of **2** > **1**. The reactivity towards BSA revealed that the quenching of BSA fluorescence by the two complexes are static quenching, and complex **2** exhibits greater binding affinity than that of complex **1**. The binding distances of **1** and **2** with BSA were calculated to be 2.92 and 3.91 nm, respectively, on the basis of the Foster's theory, which indicates the energy transfer from BSA to complexes can occur. The cytotoxic studies show that the complexes exhibit high cytotoxic activity against different cell lines tested. Also, the results of cytotoxicity revealed that the metal complexes are more effective than that of the respective free ligands under identical experimental conditions and the use of bromide instead of chloride improved the biological activity. It is interesting that the DNA and protein binding abilities of the two complexes are consistent with *in vitro* cytotoxic activity and follow the order of **2** > **1**.

4. Experimental

4.1. General

Starting materials and solvents were purchased from Sigma–Aldrich or Alfa Aesar and used without further purification. *FS*-DNA and BSA were purchased from Sigma–Aldrich and were used as supplied. Cisplatin was gifted from Isfahan University of Medical Sciences. Infrared spectra were recorded on a FT-IR JASCO 680 spectrophotometer in the spectral range 4000–400 cm^{-1} using the KBr pellets technique. NMR spectra were measured on a Bruker spectrometer at 400.13 MHz (^1H) and 161.97 MHz (^{31}P) using standard pulse sequences at 298 K. Elemental analysis was performed on a Leco, CHNS-932 apparatus. UV–Vis spectra were recorded on a JASCO 7580 UV–Vis–NIR double-beam spectrophotometer using a quartz cell with a path length of 10 mm. Fluorescence spectra were performed on a Perkin–Elmer LS55 fluorescence spectrofluorometer.

4.2. Synthesis of $[Pd_2\{(C,N)-C_6H_4CH_2NH(Et)\}_2(\mu\text{-dppe})(Cl)_2]$ (**1**)

To a suspension of the dimer $[Pd_2\{(C,N)-C_6H_4CH_2NH(Et)\}_2(\mu\text{-}Cl)_2]$ (0.077 g, 0.14 mmol) in dichloromethane (15 mL) was added dppe (0.055 g, 0.14 mmol). The reaction mixture was stirred for 2 h at room temperature and then filtered through a plug of $MgSO_4$. The filtrate was concentrated to ca. 2 mL and to this concentrated solution, *n*-hexane (15 mL) was added to precipitate a white solid, which was collected and air-dried. White crystals of **1** were obtained from CH_2Cl_2–hexane. Yield: 85%. ^1H NMR ($CDCl_3$, ppm): δ = 1.29 (t, 3H, CH_3), 2.72–2.81 (m, 1H, CH_aH), 2.85–3.20 (m, 2H, CH_2), 3.20–3.26 (m, 1H, CH_bH), 3.81–3.90 (m, 2H, CH_2 (dppe)), 4.68 (br s, 1H, NH), 6.28 (br s, 1H, C_6H_4), 6.40 (t, 1H, C_6H_4), 6.80 (t, 1H, C_6H_4), 6.98 (d, 1H, C_6H_4), 7.28–7.95 (m, 10H, Ph); $^{31}P\{^1H\}$ NMR ($CDCl_3$, ppm): δ = 37.3 (s). Anal. calcd. for $C_{44}H_{48}N_2P_2Cl_2Pd_2$: C, 55.5; H, 5.08; N, 2.94. Found: C, 55.3; H, 5.02; N, 2.90%.

4.3. Synthesis of [Pd_2{(C,N)–$C_6H_4CH_2NH(Et)$}$_2$(μ-dppe)($Br)_2$] (**2**)

To a suspension of the dimer [Pd_2{(C,N)–$C_6H_4CH_2NH(Et)$}$_2$(μ-$Br)_2$] (0.089 g, 0.14 mmol) in dichloromethane (15 mL) was added dppe (0.055 g, 0.14 mmol). The reaction mixture was stirred for 2 h at room temperature and then filtered through a plug of $MgSO_4$. The filtrate was concentrated to ca. 2 mL and to this concentrated solution, *n*-hexane (15 mL) was added to precipitate a white solid, which was collected and air-dried. Yield: 87%. ^{1}H NMR ($CDCl_3$, ppm): δ = 1.26 (t, 3H, CH_3), 2.80 (m, 1H, CH_aH), 2.89–2.99 (m, 2H, CH_2), 3.21 (m, 1H, CH_bH), 3.82–3.96 (m, 2H, CH_2 (dppe)), 4.71 (br s, 1H, NH), 6.29 (br m, 1H, C_6H_4), 6.42 (t, 1H, C_6H_4), 6.82 (t, 1H, C_6H_4), 7.01 (d, 1H, C_6H_4), 7.26–7.90 (m, 10H, Ph); ^{31}P{^{1}H} NMR ($CDCl_3$, ppm): δ = 36.7 (s). Anal. calcd. for $C_{44}H_{48}N_2P_2Br_2Pd_2$: C, 50.84; H, 4.65; N, 2.69. Found: C, 50.35; H, 4.62; N, 2.65%.

4.4. Crystallography

X-ray diffraction experiments were done at 100 K with the use of Agilent SuperNova single crystal diffractometer (Mo K(α) radiation). Analytical numeric absorption correction using a multifaceted crystal model based on expressions derived by R.C. Clark & J.S. Reid was made [75]. The structures were solved by direct methods using the SHELXS97 program and refined with the use of SHELXL (Sheldrick 2008) program. Hydrogen atoms were added in the calculated positions and were riding on their respective carbons during the refinement.

4.5. DNA-binding studies

The DNA-binding studies were performed at room temperature by electronic absorption spectrometric experiments and were conducted by adding *FS*-DNA solution to the sample of **1** and **2** at different concentrations. Fluorescence quenching experiments were conducted by adding the solutions of **1** and **2** at different concentrations to the samples containing 2 μM EB and 60 μM DNA. The samples were excited at 471 nm, and emission was recorded at 540–700 nm. All studies on the interaction of compounds with *FS*-DNA were carried out in Tris–HCl buffer (5 mM Tris–HCl/10 mM NaCl at pH 7.2). The solutions of *FS*-DNA gave a ratio of UV absorbance at 260 and 280 nm of 1.86, indicating that the DNA was sufficiently free of protein [76]. The DNA concentration per nucleotide was determined by absorption spectrometry using the known molar extinction coefficient value of 6600 M^{-1} cm^{-1}at 260 nm [77].

4.6. BSA-binding studies

All experiments involving BSA were performed in Tris–HCl buffer (5 mM Tris–HCl/10 mM NaCl at pH 7.2). Solutions of BSA were prepared by dissolving them in the Tris–HCl buffer solution to required concentrations, respectively. For UV absorption experiment, a solution of BSA (15 μM) was titrated with various concentrations of the complexes. Equal solutions of complexes were added to the reference solutions to eliminate the absorbance of the complexes themselves. In the tryptophan fluorescence quenching experiment, quenching of the tryptophan residues of BSA [78] was done by keeping the concentration of the BSA constant while varying the complexes (quenchers) concentration, producing the solutions with the varied mole ratio of the quenchers to BSA. The fluorescence spectra were recorded at an excitation wavelength of 295 nm and an emission wavelength of 343 nm in the Fluorometer after each addition of the quencher.

4.7. Cell culture and MTT assay

Hela, HT-29, K562 and MCF-7 cell lines were purchased from Pasture Institute, Tehran, Iran. They were grown in PRMI 1640 which was supplemented with 10% of fetal calf serum, 5 mL of penicillin/streptomycin (50 IU mL^{-1} and 500 μg mL^{-1}, respectively), $NaHCO_3$ (1 g) and 5 mL of L-glutamine (2 mM). Completed media was sterilized through 0.22 μm microbiological filters after preparation and kept at 4 °C before using.

The cytotoxic effects of compounds against various cell lines were determined by a rapid colorimetric assay using 3-[4,5-dimethylthiazole-2-yl]-2,5-diphenyl tetrazolium bromide (MTT) for cell growth inhibition and compared with untreated control [79]. The test is based on the reduction of the yellow tetrazolium salt MTT to a violet formazan product via the mitochondrial succinate dehydrogenase in living cells. The color can then be quantified by spectrophotometric means. The amount of violet color produced is directly proportional to the number of viable cells. Briefly 200 μL of cells (1×10^5 cells/mL) were seeded in 96-well micro plates and incubated for 24 h (37 °C, 5% CO_2 air humidified). Then, 20 μL of final concentration of each compound was added and incubated for another 72 h in the same condition. To evaluate cell survival, each well was incubated with 20 μL of MTT solution (5 mg/mL in phosphate-buffered saline) for 3 h and afterward, 150 μL of the media of each well was gently replaced with DMSO and mixed to dissolve insoluble formazan crystals. The MTT-formazan absorption was measured at 540 nm using an ELISA plate reader (Stat fax2100, Awareness, USA). The percentage of inhibition was calculated using the ratio between the absorbance of treated and untreated cells.

Acknowledgments

Funding of our research from the Isfahan University of Technology (IUT) is gratefully acknowledged.

Appendix A. Supplementary data

Supplementary data related to this article can be found at http://dx.doi.org/10.1016/j.ejmech.2013.11.042.

References

[1] P.J. Loehrer, L.H. Einhorn, Cisplatin, Ann. Int. Med. 100 (1984) 704–713.
[2] F.M. Muggia, Cisplatin update, Semin. Oncol. 18 (1991) 1–4.
[3] H.M. Pinedo, J.H. Schornagel, Platinum and Other Metal Coordination Compounds in Cancer Chemotherapy 2, Plenum Press, New York, 1996.
[4] B. Lippert (Ed.), Cisplatin: Chemistry and Biochemistry of a Leading. Anticancer Drug, VHCA/Wiley-VCH, Zürich/Weinheim, 1999.
[5] E.R. Jamieson, S.J. Lippard, Chem. Rev. 99 (1999) 2467–2498.
[6] J. Reedijk, Chem. Rev. 99 (1999) 2499–2510.
[7] D.Z. Yang, A.H.J. Wang, Prog. Biophys. Mol. Biol. 66 (1996) 81–111.
[8] L.R. Kelland, Nat. Rev. Cancer 7 (2007) 573–584.
[9] Y.P. Ho, S.C.F. Au-Yeung, K.K.W. To, Med. Res. Rev. 23 (2003) 633–655.
[10] I. Kostova, Recent Pat. Anti-Cancer Drug Discovery 1 (2006) 1–22.
[11] M.A. Jakupec, M. Galanski, B.K. Keppler, Rev. Physiol. Biochem. Pharmacol. 146 (2003) 1–53.
[12] E. Wong, C.M. Giandomenico, Chem. Rev. 99 (1999) 2451–2466.
[13] M.M. Shoukry, A.A. Shoukry, M.N. Hafez, J. Coord. Chem. 63 (4) (2010) 652–664.
[14] A.D. Ryabov, Synthesis (1985) 233–252.
[15] M. Pfeffer, Pure Appl. Chem. 64 (1992) 335–342.
[16] W.A. Herrmann, C. Brossmer, K. Ofele, C.P. Reisinger, T. Priermeier, M. Beller, H. Fischer, Angew. Chem., Int. Ed. Engl. 34 (1995) 1844–1848.
[17] K. Karami, M. Ghasemi, N. Haghighat Naeini, Tetrahedron Lett. 54 (2013) 1352–1355.
[18] K. Karami, M. Bahrami Shehni, N. Rahimi, Appl. Organomet. Chem. 27 (2013) 437–443.
[19] K. Karami, Z. Karami Moghadam, M. Hosseini-Kharat, Catal. Commun. 43 (2014) 25–28.
[20] V.I. Sokolov, Pure Appl. Chem. 55 (1983) 1837–1844.

[21] R. Schwarz, G. Gliemann, J. Jolliet, A. von Zalevsky, Inorg. Chem. 28 (1989) 742–746.
[22] R.J. Doyle, G. Salem, A.C. Willis, J. Chem. Soc., Dalton Trans. (1995) 1867–1872.
[23] J. Albert, J. Granell, G. Muller, D. Sainz, M.F. Bardia, X. Solans, Tetrahedron Asymmetry 6 (1995) 325–328.
[24] A.M.G. Godquin, P.M. Maitlis, Angew. Chem., Int. Ed. Engl. 30 (1991) 375–402.
[25] M. Ghedini, F. Neve, D. Pucci, Eur. J. Inorg. Chem. (1998) 501–504.
[26] J.D. Higgins, J. Inorg. Biochem. 49 (1993) 149–156.
[27] C. Navarro-Ranninger, J. Lopez-Solera, J.M. Perez, J.M. Massanger, C. Alonso, Appl. Organomet. Chem. 7 (1993) 57–61.
[28] M. Curic, L. j. Tusek-Bozic, D. Vikic-Topic, V. Scarcia, A. Furlani, J. Balzarini, E. De Clercq, J. Inorg. Biochem. 63 (1996) 125–142.
[29] K. Karami, M. Hosseini-Kharat, H. Sadeghi-Aliabadi, J. Lipkowski, M. Mirian, Polyhedron 50 (2012) 187–192.
[30] C. Bincoletto, I.L.S. Tersariol, C.R. Oliveira, S. Dreher, D.M. Fausto, M.A. Soufen, F.D. Nascimento, A.C.F. Caires, Bioorg. Med. Chem. 13 (2005) 3047–3055.
[31] V. Mahalingam, N. Chitrapriya, F.R. Fronczek, K. Natarajan, Polyhedron 27 (2008) 2743–2750.
[32] S. Sharma, S.K. Singh, M. Chandra, D.S. Pandey, J. Inorg. Biochem. 99 (2005) 458–466.
[33] C. Metcalfe, J.A. Thomas, Chem. Soc. Rev. 32 (2003) 215–224.
[34] C.M. Che, M. Yang, K.H. Wong, H.L. Chan, W. Lam, Chem. Eur. J. 5 (1999) 3350–3356.
[35] D.L. Ma, C.M. Che, Chem. Eur. J. 9 (2003) 6133–6144.
[36] T. Okada, I.M. El-Mehasseb, M. Kodaka, T. Tomohiro, K.I. Okamoto, H. Okuno, J. Med. Chem. 44 (2001) 4661–4667.
[37] A. Crispini, M. Ghedini, J. Chem. Soc., Dalton Trans. (1997) 75–80.
[38] M. Ghedini, I. Aiello, A. Crispini, A. Golemme, M. La Deda, D. Pucci, Coord. Chem. Rev. 250 (2006) 1373–1390.
[39] C. Navarro-Ranninger, I. Lopez-Solera, V.M. Gonzalez, J.P. Perez, A. Alvarez-Valdes, A. Martin, P.R. Raithby, J.R. Masaguer, C. Alonso, Inorg. Chem. 35 (1996) 5181–5187.
[40] F. Zamora, V.M. Gonzalez, J.P. Perez, J.R. Masaguer, C. Alonso, C. Navarro-Ranninger, Appl. Organomet. Chem. 11 (1997) 659–666.
[41] N. Wang, L. Ye, B.Q. Zhao, J.X. Yu, Braz. J. Med. Biol. Res. 41 (2008) 589–595.
[42] S. Shao, J. Qiu, Acta Phys. Chim. Sin. 25 (2009) 1342–1346.
[43] P. Martinez-Landeira, J.M. Ruso, G. Prieto, F. Sarmiento, M.N. Jones, Langmuir 18 (2002) 3300–3305.
[44] N. Zhou, Y.Z. Liang, P. Wang, J. Photochem. Photobiol., A 185 (2007) 271–276.
[45] L. Shang, X. Jiang, S. Dong, J. Photochem. Photobiol., A 184 (2006) 93–97.
[46] K. Karami, M. Hosseini-Kharat, C. Rizzoli, J. Lipkowski, J. Organomet. Chem. 728 (2013) 16–22.
[47] K. Karami, M.M. Salah, Appl. Organomet. Chem. 24 (2010) 828–832.
[48] J. Albert, R. Bosque, L. D'Andrea, J. Granell, M. Font-Bardia, T. Calvet, Eur. J. Inorg. Chem. (2011) 3617–3631.
[49] L. Pauling, The Nature of Chemical Bond, Cornell University Press, New York, 1960.
[50] E.T. de Almeida, A.E. Mauro, A.M. Santana, S.R. Ananias, A.V.G. Netto, J.G. Ferreira, R.H.A. Santos, Inorg. Chem. Commun. 10 (2007) 1394–1398.
[51] J. Spencer, R.P. Rathnam, M. Motukuri, A.K. Kotha, S.C.W. Richardson, A. Hazrati, J.A. Hartley, L. Male, M.B. Hursthouse, Dalton Trans. (2009) 4299–4303.
[52] Z.C. Liu, B.D. Wang, B. Li, Q. Wang, Z.Y. Yang, T.R. Li, Y. Li, Eur. J. Med. Chem. 45 (2010) 5353–5361.
[53] R. Prabhakaran, P. Kalaivani, P. Poornima, F. Dallemer, R. Huang, V.V. Padma, K. Natarajan, Bioorg. Med. Chem. 21 (2013) 6742–6752.
[54] A. Wolfe, G.H. Shimer, T. Meehan, Biochemistry 26 (1987) 6392–6396.
[55] R.S. Kumar, S. Arunachalam, V.S. Periasamy, C.P. Preethy, A. Riyasdeen, M.A. Akbarsha, Eur. J. Med. Chem. 43 (2008) 2082–2091.
[56] L.M. Chen, J. Liu, J.C. Chen, C.P. Tan, S. Shi, K.C. Zheng, L.N. Ji, J. Inorg. Biochem. 102 (2008) 330–341.
[57] Y.J. Hu, Y. Liu, J.B. Wang, X.H. Xiao, S.S. Qu, J. Pharm. Biomed. Anal. 36 (2004) 915–919.
[58] Y.Y. Yue, X.G. Chen, J. Qin, X.J. Yao, Dyes Pigm. 79 (2008) 176–182.
[59] H.Y. Liu, Z.H. Xu, Chem. Pharm. Bull. 57 (2009) 1237–1242.
[60] P. Kalaivani, R. Prabhakaran, M.V. Kaveri, R. Huang, R.J. Staples, K. Natarajan, Inorg. Chim. Acta 405 (2013) 415–426.
[61] T. Peters, Serum albumin, Adv. Protein Chem. 37 (1985) 161–245.
[62] S.S. Bhat, A.A. Kumbhar, H. Heptullah, A.A. Khan, V.V. Gobre, S.P. Gejji, V.G. Puranik, Inorg. Chem. 50 (2011) 545–558.
[63] S. Deepa, A.K. Mishra, J. Pharm. Biomed. Anal. 38 (2005) 556–563.
[64] M. Jiang, M.X. Xie, D. Zheng, Y. Liu, X.Y. Li, X. Chen, J. Mol. Struct. 692 (2004) 71–80.
[65] Z. Xu, G. Bai, C. Dong, Bioorg. Med. Chem. 13 (2005) 5694–5699.
[66] N. Arshad, N. Abbas, M.H. Bhatti, N. Rashid, M.N. Tahir, S. Saleem, B. Mirza, J. Photochem. Photobiol., B 117 (2012) 228–239.
[67] L.A. Sklar, B.S. Hudson, R.D. Simoni, Biochemistry 16 (1977) 5100–5108.
[68] Y.Y. Yue, X.G. Chen, J. Qin, X.J. Yao, J. Pharm. Biomed. Anal. 49 (2009) 756–759.
[69] B. Valeur, J.C. Brochon, New Trends in Fluorescence Spectroscopy, sixth ed., Springer Press, Berlin, 1999, p. 25.
[70] F.L. Cui, J. Fan, D.L. Ma, M.C. Liu, X.G. Chen, Z. Hu, Anal. Lett. 36 (2003) 2151–2166.
[71] N. Miklásová, E. Fischer-Fodor, P. Lönnecke, C.I. Tomuleasa, P. Virag, M.P. Schrepler, R. Miklás, L.S. Dumitrescu, E. Hey-Hawkins, Eur. J. Med. Chem. 49 (2012) 41–47.
[72] J. Zhang, L. Ma, H. Lu, Y. Wang, S. Li, S. Wang, G. Zhou, Eur. J. Med. Chem. 58 (2012) 281–286.
[73] L. Tusek-Bozic, M. Juribasic, P. Traldi, V. Scarcia, A. Furlani, Polyhedron 27 (2008) 1317–1328.
[74] A.C. Moro, A.E. Mauro, A.V.G. Netto, S.R. Ananias, M.B. Quilles, I.Z. Carlos, F.R. Pavan, C.Q.F. Leite, M. Horner, Eur. J. Med. Chem. 44 (2009) 4611–4615.
[75] R.C. Clark, J.S. Reid, Acta Crystallogr. A51 (1995) 887–897.
[76] J. Marmur, J. Mol. Biol. 3 (1961) 208–218.
[77] M.E. Reichman, S.A. Rice, C.A. Thomas, P. Doty, J. Am. Chem. Soc. 76 (1954) 3047–3053.
[78] N.S. Quiming, R.B. Vergel, M.G. Nicolas, J.A. Villanueva, J. Health Sci. 51 (2005) 8–15.
[79] T. Mosmann, J. Immunol. Methods 65 (1983) 55–63.